Acta Pharmaceutica Sinica B 2023;13(3):1246−1261

Chinese Pharmaceutical Association
Institute of Materia Medica, Chinese Academy of Medical Sciences

Acta Pharmaceutica Sinica B

www.elsevier.com/locate/apsb
www.sciencedirect.com

ORIGINAL ARTICLE

ROS-removing nano-medicine for navigating inflammatory microenvironment to enhance anti-epileptic therapy

Zheng Zhou, Keying Li, Yongchao Chu, Chao Li, Tongyu Zhang, Peixin Liu, Tao Sun, Chen Jiang*

Department of Pharmaceutics, School of Pharmacy, Fudan University; Key Laboratory of Smart Drug Delivery, Ministry of Education; State Key Laboratory of Medical Neurobiology and MOE Frontiers Center for Brain Science, Shanghai 201203, China

Received 22 June 2022; received in revised form 29 August 2022; accepted 15 September 2022

KEY WORDS

Epilepsy;
Polymeric micelle;
Reactive oxygen species;
Inflammation;
Gliosis;
Neuroprotection

Abstract As a neurological disorder in the brain, epilepsy is not only associated with abnormal synchronized discharging of neurons, but also inseparable from non-neuronal elements in the altered microenvironment. Anti-epileptic drugs (AEDs) merely focusing on neuronal circuits frequently turn out deficient, which is necessitating comprehensive strategies of medications to cover over-exciting neurons, activated glial cells, oxidative stress and chronic inflammation synchronously. Therefore, we would report the design of a polymeric micelle drug delivery system that was functioned with brain targeting and cerebral microenvironment modulation. In brief, reactive oxygen species (ROS)-sensitive phenylboronic ester was conjugated with poly-ethylene glycol (PEG) to form amphiphilic copolymers. Additionally, dehydroascorbic acid (DHAA), an analogue of glucose, was applied to target glucose transporter 1 (GLUT1) and facilitate micelle penetration across the blood−brain barrier (BBB). A classic hydrophobic AED, lamotrigine (LTG), was encapsulated in the micelles *via* self-assembly. When administrated and transferred across the BBB, ROS-scavenging polymers were expected to integrate anti-oxidation, anti-inflammation and neuro-electric modulation into one strategy. Moreover, micelles would alter LTG distribution *in vivo* with improved efficacy. Overall, the combined anti-epileptic therapy might provide effective opinions on how to maximize neuroprotection during early epileptogenesis.

*Corresponding author. Tel.: +86 021 51980079.
E-mail address: jiangchen@shmu.edu.cn (Chen Jiang).

Peer review under the responsibility of Chinese Pharmaceutical Association and Institute of Materia Medica, Chinese Academy of Medical Sciences

https://doi.org/10.1016/j.apsb.2022.09.019

1. Introduction

Epilepsy, characterized by recurrent, unpredictable seizures, is a neurological disorder in the brain triggered by abnormal synchronized discharging of populations of neurons. Apart from imbalanced neurotransmissions, however, more pathological factors are recently found to get involved in epileptogenesis, including reactive gliosis, oxidative stress and chronic inflammation[1,2]. During epileptogenesis, there could be a valuable time window to restrict molecular or cellular pathology in the brain, especially that of impaired neurons and activated neuroglia. Activity of inflammation is elevated during oxidative stress, and clearance of ROS could remodel immunologic microenvironment to depress epileptogenesis[3,4]. Therefore, antioxidants (*e.g.*, bioactive enzymes and natural chemical components) and anti-epileptic drugs (AEDs) could probably be exploited together as upgraded therapies for synchronous modulation of inflammatory microenvironment and abnormal neural activities[5,6].

Unfortunately, there have been few reports of strategies navigating inflammatory pathways for early involvement in epileptogenesis in previous studies generally[7,8]. What's worse, bioactive enzymes or natural chemicals, for one thing, suffer from the challenge of penetrating the blood–brain barrier (BBB) when delivered *in vivo* for cerebral diseases; for another, they would fail to accumulate in epileptic lesions after entering the central nervous system (CNS)[9]. Therefore, traditional AEDs are still commonly applied as the main treatment of epilepsy in clinic[10–12]. Nevertheless, conventional AEDs normally focus on ion channels in the CNS, falling short in abating oxidative stress or inflammatory response. Thus, they result in unsatisfying anti-epileptic effects[13]. Exactly, about 30% of epileptic patients have expressed resistance against conventional AEDs, who have little choice but progress to refractory epilepsy[14].

Therefore, novel ROS-reactive elements are necessary to function as a due compensation for the deficiencies mentioned above. They are expected to specifically respond to the stimulation of pathologically high concentration of ROS [*e.g.*, superoxide ($O_2\cdot^-$), hydrogen peroxide (H_2O_2), peroxynitrite ($ONOO^-$) and hypochlorous acid (HOCl)], and achieve smart accumulation in epileptic foci[15]. From different ROS-responsive groups, arylboronic acid and ester stand out because of a unique 1,6-elimination process: they are highly sensitive to oxidation by ROS, H_2O_2 in particular, and generate harm-free final products, phenols and boronic acid[16,17] (Fig. 1A). Recently, polymers modified with sidechains containing arylboronic acid and ester are frequently reported, where ROS-stimulation can covert the polymer's hydrophobicity into hydrophilicity, triggering the degradation of the drug delivery system (DDS) and the release of encapsulated drugs[18,19]. Therefore, arylborate ester was selected here as the ROS-sensitive and scavenging group in our ROS-responsive DDS.

Besides, adverse drug reactions (ADRs) during long-term administration and susceptibility to relapse are other problems facing AEDs. These problems can be attributed to high drug dosages needed for adequate efficacy in the CNS, which lead to nonselective effects on the peripheral. LTG, a second-generation AED, has reduced ADRs in comparison with first-generation AEDs, but its hydrophobicity restricts the effective concentration *in vivo*[20,21]. To attain enhanced accumulation in brain and reduced dose-dependent ADRs, we designed a nano-DDS to encapsulate LTG for improved drug delivery efficiency[22]. Considering good flexibility of nano-medicines for surface modification, we selected a reported analogue of glucose, DHAA (compound 15 in Supporting Information Scheme S1), to decorate the surface of nano-medicine, which would be transported by GLUT1 on the blood–brain barrier (BBB)[23–25].

It is reported that the brain is a highly energy-demanding organ and glucose is the preferred energy substrate[26]. Under physiological conditions, neurons derive almost all of their energy from the aerobic oxidation of glucose. As a nutrient transporter and energy capture channel, GLUT1 is highly expressed in the BBB cells and isolated brain vessels[23]. GLUT1 is responsible for transporting hexoses such as glucose into the brain, which will then be utilized by neurons[24]. During epilepsy, abnormal electric activities and hyper-excitability of neurons in epileptic foci (mainly in hippocampus) will consume more energy, resulting in larger demand of glucose[27,28]. Besides, polymeric micellar nanocarriers conjugated to multiple glucose molecules have been reported to cross the BBB for drug delivery into the brain[23]. Therefore, glucosylated nanocarriers transported by GLUT1 into the brain is expected to become a breakthrough point for targeting epileptic foci. As an analogue of glucose, DHAA is selected as the targeting ligand, which has been reported to be recognized by GLUT1 and transported into the brain like glucose[24,25]. Thus DHAA-modified nano-medicine is expected to enhance BBB permeability and facilitate cerebral accumulation.

Herein, a self-assembly polymeric micelle system (LTG encapsulated in DHAA-PEG-poly-LysB, abbre*via*ted LTG@DPLB) with brain-targeting and ROS-responsive functions was reported. Arylboronate ester, as the hydrophobic sidechain, also served to dissolve LTG based on the principle of "like dissolves like". Meanwhile, the hydrophilic sidechain comprising PEG would slow down clearance by reticuloendothelial system (RES) in circulation[29]. After crossing the BBB mediated by DHAA, the nano-medicine would degrade under anomalously increased ROS in epileptic foci and release LTG to arrest aberrant neural firing (Fig. 1B). Moreover, ROS-clearance based on ROS-scavenging polymers (mPEG-poly-LysB or DHAA-PEG-poly-LysB, abbreviated PLB or DPLB) would further prevent the progress of oxidative stress and chronic inflammation, contributing to the stability of glia. In summary, we wish to integrate anti-oxidation, anti-inflammation and neuro-electric modulation into one strategy as a combined anti-epileptic therapy to maximize neuroprotection and glia-resting during early epileptogenesis (Scheme 1).

2. Materials and methods

2.1. Synthesis and ROS-induced degradation of polymeric monomers

Detailed steps of chemical synthesis are shown in Supporting Information Scheme S1. All synthesized products were characterized by ^{1}H NMR spectra (400 MHz, Oxford Instruments, Abingdon, UK) or mass spectra (ESI, Thermo Fisher Scientific, Waltham, MA, USA).

To confirm the ROS-sensitivity of polymeric materials (PLB and DPLB), they were dissolved in little methanol and then diluted to 400 μg/mL with PBS 7.4 or PBS 7.4 containing 100 μmol/L H_2O_2. The solution was incubated at 37 °C while samples were taken every 30 min and 100 μmol/L H_2O_2 was added every 2 h. The concentration of 4-hydroxybenzyl alcohol was determined by high performance liquid chromatography (HPLC, Agilent Technologies, Santa Clara, CA, USA). In the end, excessive H_2O_2 was added to completely decompose phenylboronic ester into 4-hydroxybenzyl alcohol, whose total

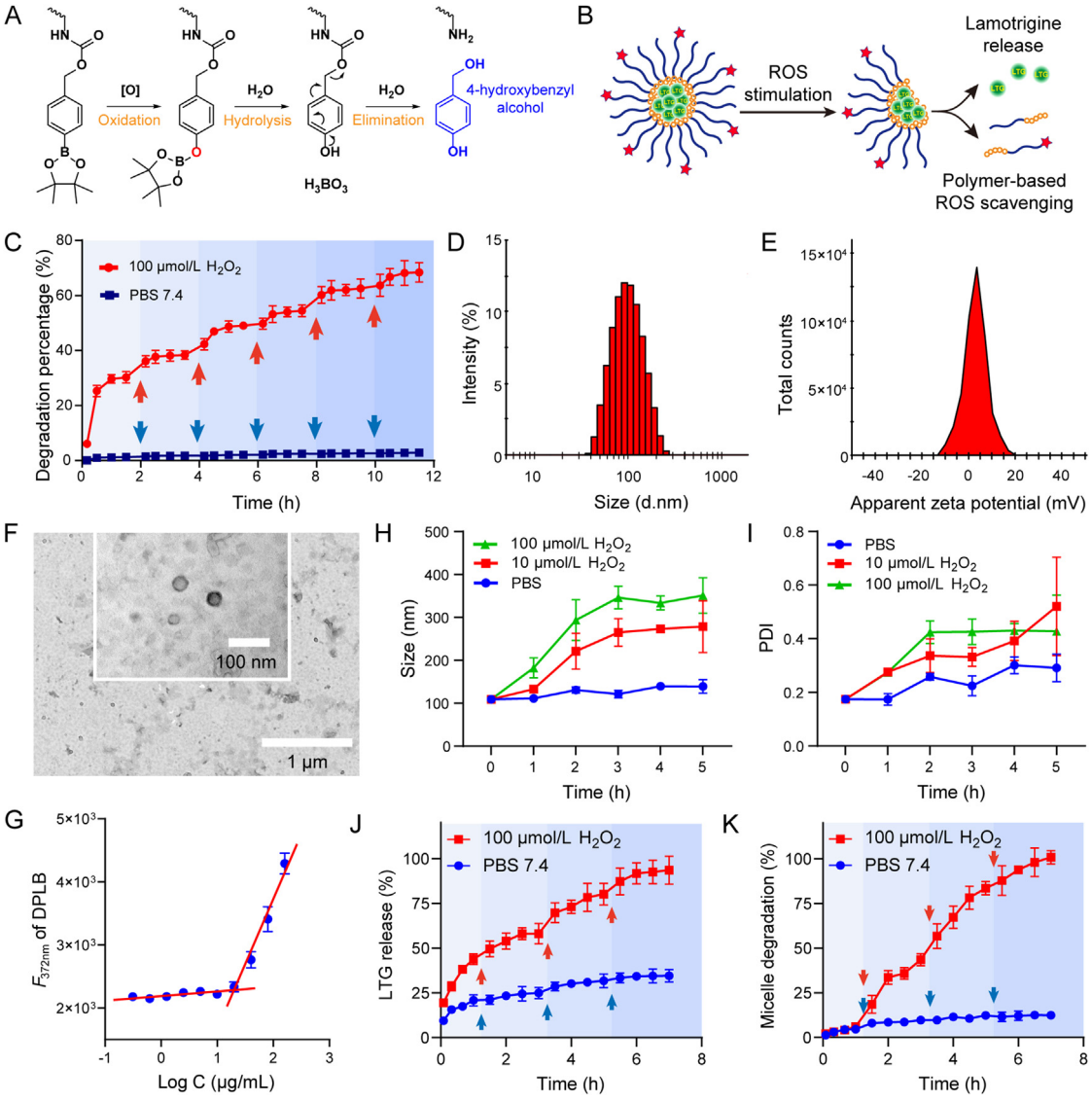

Figure 1 Preparation and characterization of micelles. (A) Degradative mechanism of the polymeric monomer (PLB or DPLB) under oxidative environment; (B) Illustration of LTG@DPLB micelle formation, degradation and drug release triggered by ROS; (C) Kinetics of polymer degradation in PBS 7.4 with or without 100 μmol/L H_2O_2. Red arrows indicate supplemental H_2O_2 to sustain the reaction and blue arrows indicate supplemental PBS. Results are presented as mean ± SD (n = 3); (D,E) Size distribution, PDI and ζ-potential of micelles measured by DLS machine; (F) Morphology of LTG@DPLB micelles measured by transmission electron microscope (TEM, scale bar: 1.0 μm; inset scale bar: 100 nm); (G) Critical micelle concentration (CMC) measurement of DPLB materials. Data are reported as mean ± SD (n = 3); (H,I) Size distribution and PDI of LTG@DPLB micelles after incubation with different concentrations of H_2O_2. Results are reported as mean ± SD (n = 3); (J,K) Dynamics of LTG release and micelle degradation of LTG@DPLB micelles in PBS 7.4 with or without 100 μmol/L H_2O_2. Red and blue arrows indicate supplemental H_2O_2 and PBS to compensate the sampling volume. Results are presented as mean ± SD (n = 3).

amount was calculated and set as 100% for degradation ratio calculation. HPLC method was optimized as below: Agilent C18 column, 250 mm × 4.6 mm; 1.0 mL/min, 10% methanol +90% H_2O (containing 0.1% *v/v* trifluoroacetic acid); injection volume, 10 μL; DAD scan wavelength, 220 nm; DAD reference wavelength, 360 nm.

2.2. *Preparation and characterization of micelles*

Polymeric micelles were prepared by thin-film rehydration method. Three kinds of micelles, empty targeted micelles (DPLB), non-targeted drug-loaded micelles (LTG@PLB) and targeted drug-loaded micelles (LTG@DPLB), were designed and prepared. They were made from PLB mixed with DPLB, PLB mixed with LTG, and PLB mixed with DPLB and LTG, respectively. All prepared liquids were filtered by 0.22 μm membrane (Whatman, Maidstone, UK) for further characterization. The nano-particle size distribution, polydispersity index (PDI) and ζ-potential were measured by dynamic light scattering (DLS) machine (Zetasizer Nano-ZS, Malvern Panalytical, Malvern, UK). All of these indexes were tested again after 7-day standing at room temperature (r.t.) to check their stability. Micelle solutions were viewed by transmission electron microscope (TEM, performed by Servicebio, Wuhan, China) to reveal the appearance of micelles.

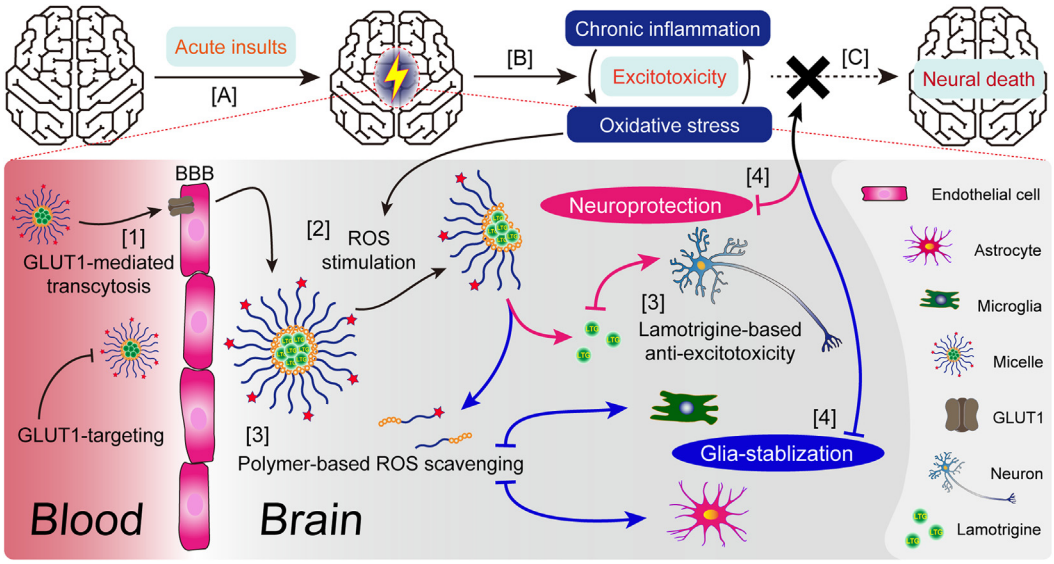

Scheme 1 Illustration of epileptogenesis, LTG-loaded micelle formation and regulation of pathological microenvironment in epileptic foci. The gradual transformation from a formerly healthy brain into one suffering from autonomous seizures, named epileptogenesis, can be divided into three phases: (A) First, a serious insult, for example, stroke or head trauma, initiates molecular and cellular changes in the affected brain regions. (B) Second, within those foci, glial cells are pathologically activated (*i.e.*, gliosis) to establish inflammatory microenvironment and release cytokines, chemokines, growth factors and other molecules to reduce or repair brain damages. However, unrestrained reactive gliosis may cause excessive inflammation, neuronal death and tissue damage and last until acute, unprovoked seizures occur. (C) Third, after continuous inflammation and recurring seizures, molecular and cellular changes can hardly be reversed and give rise to neural death. Our nano-medicine will (1) penetrate the BBB with the help of GLUT1-targeting ligand DHAA and then (2) release lamotrigine under the stimulation from high concentration of ROS in epileptic lesions. (3) Lamotrigine is delivered to prevent aberrant firing while ROS-scavenger phenylboronic ester can reduce oxidative stress to alleviate chronic inflammation. (4) Finally, epileptogenesis will hopefully be terminated due to our nano-medicine's protection to neurons and stabilizing effect on glia.

The critical micelle concentration (CMC) of PLB and DPLB was measured by pyrene fluorescence probe spectrometry. Micelle solutions of PLB or DPLB with different concentrations (calculated by materials) were incubated with dry pyrene at r.t. overnight. The fluorescence intensity was measured at 372 nm by a microplate reader (BioTek Instruments, Winooski, VT, USA) and plotted vs micelle concentrations. Linear regression was applied to form two linear parts and CMC was determined as the abscissa value of the intersection of these two lines.

LTG-loaded micelles were diluted with methanol and disrupted to release LTG completely, whose concentration was determined as total LTG by HPLC. Ultrafiltration (10 kDa MWCO, Beyotime, Shanghai, China) was applied to separate free LTG from micelle solutions, while lyophilization was utilized to confirm the total weight of micelles. Encapsulation efficiency (EE, %) and drug loading (DL, %) were calculated according to the following Eqs. (1) and (2):

$$\text{EE}\ (\%) = (\text{Total LTG} - \text{Free LTG}) / \text{Total LTG} \times 100 \quad (1)$$

$$\text{DL}\ (\%) = (\text{Total LTG - Free LTG}) / \text{Total weight of micelles} \times 100 \quad (2)$$

HPLC method was optimized as below: Agilent C18 column, 250 mm × 4.6 mm; 1.0 mL/min, 40% methanol + 60% H_2O (containing 0.1% *v/v* trifluoroacetic acid); injection volume, 10 μL; DAD scan wavelength, 220 nm; DAD reference wavelength, 360 nm.

2.3. *ROS-sensitive degradation and drug-release of micelles*

To confirm the ROS-sensitivity of micelles, LTG@DPLB was diluted in PBS 7.4 containing 0, 10 or 100 μmol/L H_2O_2 and incubated at 37 °C. The particle size and PDI of micelle solutions were measured every 1 h. Furthermore, LTG@DPLB solution was placed in a dialysis bag which was then soaked in PBS 7.4 or PBS 7.4 containing 100 μmol/L H_2O_2. The solution was incubated at 37 °C while samples were taken every 15 min and 100 μmol/L H_2O_2 was added every 1 h. The concentration of 4-hydroxybenzyl alcohol and LTG were determined by HPLC with the same methods as mentioned before.

2.4. *Cell lines*

Brain capillary endothelial cells (BCECs), sharing common characteristic with the BBB, were cultured in Dulbecco's modified Eagle's medium (DMEM, Thermo Fisher Scientific) containing 20% heat-inactivated fetal bovine serum (FBS, Gibco, Waltham, MA, USA), 100 mg/L epidermal cell growth supplement (Thermo Fisher Scientific), 300 mg/L L-glutamine, 20 mg/L heparin, 100 U/mL penicillin and 100 mg/L streptomycin (Meilunbio, Dalian, China). Specially, all the culture dishes or inserts for BCECs were coated with gelatin (2% in H_2O) before usage. SH-SY5Y cells (human neuroblastoma) were grown in DMEM: F-12 (DMEM/F-12, Thermo Fisher Scientific) containing 10% FBS, 100 U/mL penicillin and 100 mg/L streptomycin. All cells were incubated at 37 °C under the condition of 5% CO_2 and saturating humidity.

2.5. Cellular biocompatibility of polymers

PLB or DPLB was dissolved in little dimethyl sulfoxide (DMSO) and then diluted with DMEM, while DHAA was directly diluted because of its hydrophilicity. SH-SY5Y cells were seeded in 96-well plate and then treated with different concentrations of PLB, DPLB or DHAA for 24 h. Cellular viability was tested by Cell Counting Kit-8 (Meilunbio).

2.6. Cellular uptake of micelles

Above all, BCECs and SH-SY5Y cells were cultured in confocal culture dishes (Corning, Corning, NY, USA) for immunofluorescence staining to simply observe their GLUT1 as a membrane protein (anti-GLUT1 antibody, 1:600, ab115730, Abcam, Cambridge, UK; goat anti-rabbit IgG Alexa Flour 488, 1:1000, ab150077, Abcam). Cells were observed under the confocal fluorescence microscope (Carl Zeiss AG, Oberkochen, Germany) with a 63 × oil immersion lens. Also, BCECs and SH-SY5Y cells were split to extract proteins and their GLUT1 expression were measured by Western blot (anti-GLUT1 antibody, 1:10,000, ab115730, Abcam; biotin-labeled goat anti-rabbit IgG, 1:1000, Beyotime).

PLB was mixed with DPLB in different weight proportions to prepare micelles with different DHAA modification ratio (0%, 10%, 20%, 40%, 80%, 100%), where coumarin-6 (Cou-6) was encapsulated as a hydrophobic and high-sensitivity fluorescence probe (E_x = 466 nm, E_m = 504 nm). The concentration of Cou-6 in micelles was measured by a microplate reader so that it would be diluted into 1 μg/mL with DMEM. BECEs or SH-SY5Y cells were cultured in 24-well plate, incubated with Cou-6-loaded micelles for 30 min and then gently washed with Hank's Balanced Salt Solution (Hank's). Finally, they were observed under a fluorescence microscope (Olympus, Tokyo, Japan). Specifically, the cytotoxicity of targeted micelle (LTG@DPLB, prepared according to the most suitable modification ratio) and non-targeted micelle (LTG@PLB) was further evaluated by the same procedure as polymers in the previous paragraph.

To reveal the internalization mechanisms of micelles, BECEs or SH-SY5Y cells were cultured in 6-well plate at a density of 1×10^5 cells per well and fed until 80% confluence was achieved. Cells were then pre-incubated under different inhibitive conditions, that were, Hank's containing phenylarine oxide (PhAsO, 1 μg/mL), colchicine (2 μg/mL), filipin (2 μg/mL) or DHAA (50 μg/mL, in massive excess) respectively for 30 min, followed by addition of LTG@DPLB (10 μg/mL LTG) and incubation for 1 h at 37 or 4 °C. Cells were gently washed and split with RIPA Lysis Buffer (Beyotime). Cellular lysates were collected to extract intracellular LTG with ethyl acetate, volatilize under N_2 and redissolve in methanol for HPLC quantification *via* the same method as mentioned before. Blank cells were also collected and processed to verify the specificity and recovery rate of HPLC method.

To investigate intracellular ROS-induced release of micelles, SH-SY5Y cells were cultured in confocal culture dishes (Corning). All dished were incubated with Cou-6-loaded micelles (20% modification) for 30 min and then gently washed with Hank's. After wash, some of the dishes were further incubated with or without 100 μmol/L H_2O_2 for another 60 min and then went through another wash. Meanwhile, all dished were incubated with Hoechst 33342 (1 μg/mL, Thermo Fisher Scientific) and LysoTracker Deep Red (50 nmol/L, Thermo Fisher Scientific) for 30 min to locate nuclei and late endosomes/lysosomes, respectively, before observation. After staining and wash, all dishes were observed under the confocal fluorescence microscope (Carl Zeiss AG) with a 63 × oil immersion lens.

To investigate the BBB permeability of micelles, BCECs were seeded into a 0.4 μm Transwell insert (NEST, Wuxi, China) at a density of 1.5×10^4 cells to form a monolayer as a brief *in vitro* BBB model. Cells of the Transwell system were cultured for about 10 days and then treated with LTG@PLB, LTG@DPLB or LTG@DPLB (10 μg/mL LTG) along with DHAA (50 μg/mL, in massive excess) while samples under the inserts were taken at the 5th, 10th, 15th and 30th min. Concentrations of LTG were measured by HPLC *via* the same method as mentioned before. ^{14}C-Labelled sucrose (Amersham Biosciences, Piscataway, NJ, USA) was selected as a permeable tracer and added through the same procedure as micelles to verify the permeability of the BBB model before and after treatment. Concentrations of ^{14}C-labelled sucrose were measured by liquid scintillation counting technique. The apparent permeability coefficients (Papp) of LTG or ^{14}C-labelled sucrose was calculated as reported before as Eq. (3):

$$P_{app} = (dQ/dt)/(C_0 \times S) \quad (3)$$

where dQ/dt was the permeability rate (nmol/s), C_0 was the primary concentration (nmol/mL) in the Transwell insert and S was the membrane area (0.33 cm^2) of the Transwell insert.

2.7. Cellular protective effects of micelles

Two different neurotoxic models were established to study cellular protective effects of micelles. In the first model, SH-SY5Y cells were cultured in 96-well plate at a density of 5000 cells/well and fed until 60% confluence was achieved. Cells were incubated with free LTG, empty DPLB, LTG@PLB and LTG@DPLB at an identical LTG concentration of 10 μg/mL for 1 h and then gently washed, followed by incubation with DMEM containing 100 μmol/L H_2O_2 for 12 h. The medium was refreshed every 4 h. Cellular viability was tested by Cell Counting Kit-8. Cells without 100 μmol/L H_2O_2 treatment served as control while cells without drug incubation served as blank group.

In the other model, SH-SY5Y cells were cultured in 6-well plate at a density of 1×10^5 cells per well and fed until 60% confluence was achieved. Cells were incubated with free LTG, empty DPLB, LTG@PLB and LTG@DPLB at an identical LTG concentration of 10 μg/mL for 1 h and then gently washed, followed by incubation with DMEM containing 50 mmol/L glutamate for 24 h to induce excitotoxicity.

Cells of some plates were gently washed and further incubated with 2′,7′-dichlorodihydrofluorescein diacetate (DCFH-DA, Energy Chemical, Shanghai, China) as an ROS-indicative probe (10 μmol/L in Hank's) for 30 min and finally observed under a fluorescence microscope. Cells of other plates were carefully dispersed, collected and stained with Annexin V-FITC (Thermo Scientific) and propidium iodide (PI, Thermo Scientific) for 15 min. Cells were then analyzed by flow cytometry (Beckman, Brea, CA, USA) for apoptosis assay.

To investigate cellular excitability after incubation with 50 mmol/L glutamate and drug treatment, cells of some plates were tested by the whole-cell patch-clamp technique (HEKA, Reutlingen, Germany). Current clamp recording mode was set at 600, 800 and 1000 pA and conducted in external solution (artificial extracellular fluid; 150 mmol/L NaCl, 5 mmol/L KCl,

2.5 mmol/L $CaCl_2$, 10 mmol/L HEPES and 10 mmol/L glucose; adjusted to pH 7.4 by NaOH). The micropipette was filled with an internal solution (artificial intracellular fluid; 8 mmol/L NaCl, 145 mmol/L KCl, 1 mmol/L $MgCl_2$ and 10 mmol/L HEPES; adjusted to pH 7.4 by KOH).

To further verify our targeted delivery strategy based on GLUT1-mediated transport of DHAA, we examined LTG@DPLB uptake in hyperexcited SH-SY5Y cells. After incubation with 50 mmol/L glutamate for 24 h, SH-SY5Y cells were then pre-incubated with DHAA (50 μg/mL, in massive excess) for 30 min, followed by addition of LTG@DPLB (10 μg/mL LTG) and incubation for 1 h at 37 °C. Intracellular LTG was collected and analyzed by HPLC with the same methods as mentioned before. Also, the expression of GLUT1 in SH-SY5Y cells treated with or without glutamate was measured by Western blot.

2.8. Animals and epileptic models

Male SD rats (280−300 g) were provided by the Experimental Animals Department of Fudan University. All animal trails were carried out in conformity with guidelines evaluated and approved by Fudan University Institutional Animal Care and Use Committee (IACUC). Acute seizure models were established *via* classic lithium-pilocarpine-induced kindling. Briefly, rats received an intraperitoneal injection (i.p.) of lithium chloride (127 mg/kg) and after 1 day (−)-scopolamine hydrobromide trihydrate (1 mg/kg) was intraperitoneally administered to rats to antagonize peripheral cholinergic effects of pilocarpine (30 mg/kg), which was intraperitoneally administered 1 h later. The behaviors of model rats were observed and graded according to Racine's classification scale. After 30 min, if scale Ⅳ or Ⅴ was not obtained, pilocarpine (10 mg/kg) would be supplemented to the rats every 30 min until status epilepticus (SE) was successfully induced. During SE, model rats were further confirmed by electroencephalogram (EEG) recording system (TECHMAN, Chengdu, China). Model rats would not be tranquilized with pentobarbital sodium (30 mg/kg) until SE lasted for 30 min.

2.9. In vivo distribution and brain-targeting efficiency of micelles

BODIPY dye (BODIPY-NH_2, Ex = 630 nm, Em = 650 nm, Thermo Fisher Scientific) was encapsulated in micelles as a hydrophobic, highly penetrable and near infrared fluorescence probe (E_x = 630 nm, E_m = 650 nm). The concentration of BODIPY in micelles was measured by HPLC so that it would be diluted into 250 μg/mL with saline. HPLC method was optimized as below: Agilent C18 column, 250 mm × 4.6 mm; 1.0 mL/min, 70% acetonitrile +30% H_2O (containing 0.1% *v/v* trifluoroacetic acid); injection volume, 10 μL; fluorescence detector; E_x = 630 nm, E_m = 650 nm. BODIPY-loaded micelles were intravenously injected (i.v.) *via* tail vein with an identical concentration of BODIPY (1 mg/kg) to epileptic rats. During the next 24 h, rats were anesthetized and visualized under IVIS® imaging system (Caliper PerkinElmer, Waltham, MA, USA) every other hour. BODIPY fluorescence intensity of head was quantified by IVIS.

To confirm cerebral distribution of micelles, more rats were intravenously administered with BODIPY-loaded micelles (1 mg/kg). At the 8th h post-injection, rats were anaesthetized and transcardially perfused with saline and 4% paraformaldehyde. Brains were wholly removed to prepare frozen coronal sections of 10 μm in thickness. For immunofluorescence staining, slices were incubated with primary antibodies (anti-CD34 antibody, 1:50, AF1387, Beyotime) and then secondary antibodies (goat anti-rabbit IgG Alexa Flour 488, ab150077, Abcam) for scanning fluorescence microscope imaging (Olympus). Meanwhile, DAPI (Beyotime) was applied to direct nuclei.

To further investigate *in vivo* distribution, epileptic rats were intravenously administered with LTG-loaded micelles (10 mg/kg). At the 8th h post-injection, they were anaesthetized and transcardially perfused only with saline to gather brains and major organs (heart, liver, spleen, lung and kidney). In particular, brains were carefully dissected to separate hippocampus. All of them were split with RIPA Lysis Buffer. Tissue lysates were collected, mixed with methanol and centrifuged to produce LTG-containing supernatant for HPLC quantification. The percentage of the injected dose per gram of tissue (ID/g of tissue, %) in different organs was calculated according to HPLC results respectively, as shown in Eq. (4):

$$\text{ID/g of tissue (\%)} = \text{LTG dose per gram of tissue} / \text{Totally injected LTG dose} \times 100 \quad (4)$$

Blank tissues were also collected and processed to verify the specificity and recovery rate of HPLC method. HPLC method was optimized as below: Agilent C18 column, 250 mm × 4.6 mm; 1.0 mL/min, 70% methanol +30% H_2O (containing 0.1% *v/v* trifluoroacetic acid); injection volume, 10 μL; VWD detector wavelength, 220 nm.

2.10. In vivo anti-epileptic efficacy of micelles

A total of 100 epileptic rats were randomly divided into 5 groups (20 rats per group) and intravenously injected with saline, free LTG, empty DPLB (equivalent amount of polymer to LTG@DPLB), LTG@PLB and LTG@DPLB (identical LTG dosage as 10 mg/kg) respectively in Days 1, 3, 6 and 10 after modeling. Weight of rats was recorded synchronously during the medication. One day after each administration, 2 rats of each group were sacrificed to prepare frozen sections for Nissl's staining and immunofluorescence staining while the other 3 rats were sacrificed to extract hippocampus and cortex homogenate for Western blot and enzyme-linked immunosorbent assay (ELISA). After Day 10, rats' behaviors of the last group were further examined by open-field test before sacrifice. Meanwhile, rats of Day 10 were processed to collect major organs for immunohistological staining.

2.10.1. Open-field test

Briefly, rats were removed from their home cage by the tail and placed directly into the left center of a black wooden shelter, where travel distance of rats within 1 min were recorded by the camera and automatically calculated by the software, Mouse Track Application (version 1.0, Stoelting Co., Wood Dale, IL, USA). Lights and background noise were strictly controlled.

2.10.2. Nissl's staining and immunofluorescence staining

In brief, rats were anaesthetized and transcardially perfused with saline and 4% paraformaldehyde. Brains were wholly removed to prepare frozen coronal sections of 10 μm in thickness. For Nissl's staining, slices were incubated with Nissl's staining solution (Beyotime) for 30 min at 37 °C and gently washed with PBS 7.4 for scanning microscope imaging (Olympus). For

immunofluorescence staining, slices were incubated with primary antibodies (anti-Iba1 antibody, 1:200, ab5076, Abcam; anti-GFAP antibody, 1:4000, ab7260, Abcam) and then secondary antibodies (donkey anti-goat IgG Alexa Flour 488, ab150129, Abcam; donkey anti-rabbit IgG Alexa Flour 555, ab150062, Abcam) for scanning fluorescence microscope imaging (Olympus). Meanwhile, DAPI (Beyotime) was applied to direct nuclei.

2.10.3. *Western blot and ELISA*

For hippocampus and cortex homogenate, rats were anaesthetized and transcardially perfused only with saline. Brains were carefully removed and dissected to separate hippocampus and cortex, which were then split with RIPA Lysis Buffer. Protein concentration of homogenate was measured by BCA Protein Assay Kit (Beyotime) to prepare samples at the same concentration for Western blot (10% SDS-PAGE, 40 μg total proteins). Targeted strips were incubated with primary antibodies (anti-NF-κB p65 antibody, ab16502, Abcam; anti-NF-κB pp65 antibody, ab86299, Abcam; β-actin mouse monoclonal antibody, Beyotime) and then secondary antibodies (biotin-labeled goat anti-rabbit IgG, Beyotime; biotin-labeled goat anti-mouse IgG, Beyotime), followed by visualization with Immobilon Western HRP Substrate (Merck, Darmstadt, Germany). IL-1β and TNF-α in the homogenate were analyzed by ELISA (Rat IL-1β/IL-1F2 DuoSet ELISA, DY501, R&D, Minneapolis, MN, USA; rat TNF-α DuoSet ELISA, DY510, R&D) according to kit instructions.

2.10.4. *Immunohistological staining*

Rats were anaesthetized and transcardially perfused with saline and 4% paraformaldehyde to collect major organs and then prepare sections of 10 μm in thickness for hematoxylin and eosin (H&E) staining.

2.11. *Statistical analysis*

Results were analyzed by GraphPad Prism 9.1.1 and presented with mean ± standard deviation (SD). The statistical significance was evaluated by *t* tests or one-way ANOVA. P value < 0.05 was considered statistically significant.

3. Results and discussion

3.1. *Synthesis and ROS-induced degradation of polymeric monomers*

Two kinds of block copolymers in the form of PEG-poly-(lysine-phenylboronic ester) (PEG-pLysB) were successfully constructed following the designed synthetic routes (Scheme S1), where all synthesized products were characterized by ^{1}H NMR spectra or mass spectra (Supporting Information Figs. S1−S11). The molecular weight ratio of hydrophilic group to hydrophobic side is calculated to be around 1:1.2[30,31]. DHAA, a glucose analogue targeting the GLUT1 on the BBB, was linked to the azide (N_3) end of the amphiphilic polymer through click reaction, in order to increase cerebral permeability. ^{1}H NMR spectra confirmed the formation of triazole, indicating a successful coupling reaction between DHAA and N_3-PEG-pLysB (Fig. S11).

Next, we evaluated the ROS-response of the synthesized polymers. 100 μmol/L H_2O_2 was selected to simulate oxidative stress in epilepsy foci since H_2O_2 is one of the most representative ROS at the pathological level *in vivo*[17,32,33]. The degradative process of PLB or DPLB under oxidative environment[34] is shown in Fig. 1A. The reaction product, 4-hydroxybenzyl alcohol[35], was selected as a degradation marker of the polymeric monomer to indicate its ROS-sensitivity (Supporting Information Fig. S12A). In PBS 7.4 without H_2O_2, HPLC did not detect the peak of degradation product within 12 h, which validated the polymer's stability. However, in PBS 7.4 containing 100 μmol/L H_2O_2, the degradation of materials enhanced over time (Fig. 1C). Each time 100 μmol/L H_2O_2 was supplied, the degradation curve exhibited a stair-like rise, and reached a plateau after about 2 h. The next time 100 μmol/L H_2O_2 was added, a stair-like rise would appear again, revealing the polymeric materials' sensitively ROS-responsive degradation.

3.2. *Preparation and characterization of micelles*

Three types of micelles, empty targeted micelles (DPLB), non-targeted drug-loaded micelles (LTG@PLB) and targeted drug-loaded micelles (LTG@DPLB), were then prepared. Dynamic light scattering (DLS) results showed that LTG@DPLB micelles had a particle size of 93.38 ± 1.963 nm, polydispersity index (PDI) of 0.112 ± 0.021 and ζ-potential of 3.020 ± 0.578 mV (Fig. 1D and E). The size distribution, PDI and ζ-potential of DPLB and LTG@PLB micelles were also measured following the same procedure (Fig. S12B). Through TEM, both DPLB and LTG@DPLB micelles appeared to be spherical, with diameters decreasing to 40 nm due to the absence of hydration shells (Fig. 1F and S12D). Drug loading (DL%) and encapsulation efficiency (EE%) were calculated to be 4.91 ± 0.74% and 77.56 ± 6.24%, respectively, for the LTG@DPLB micelles, and 5.31 ± 0.55% and 82.21 ± 2.58%, respectively, for LTG@PLB micelles. Seven days of stability test saw an observable but acceptable increase in the particle size and PDI, while ζ-potential remained stable throughout (Fig. S12C). CMC was measured to avoid undesirable disassembly in the blood circulation, which turned out to be 20.57 μg/mL for PLB, and a slightly higher 28.65 μg/mL for DPLB (Fig. 1G and S12E). As the amphiphilic polymers were rehydrated to form emulsions of 4 mg/mL, the micelles should stay intact even when diluted 100 times.

The ROS-sensitive degradation of the micelles was also examined. Particle size and PDI of the micelles increased over time under ROS stimulation, while remained constant in PBS 7.4 without H_2O_2 (Fig. 1H and I). Thus, we concluded that the micelles were able to respond sensitively to the rise of ROS concentration by accelerated degradation. Furthermore, the concentration of LTG and 4-hydroxybenzyl alcohol was measured by HPLC (Fig. S12F) to monitor drug release and polymeric degradation, respectively. It was observed that the stimulation of ROS lead to more rapid drug release (Fig. 1J). Moreover, with the addition of H_2O_2 at regular intervals, the micelles remained ROS-sensitive, triggering fluxes of drug release before reaching a plateau again (Fig. 1K). Under constant ROS stimulation, the polymers, which kept stable in plain PBS, would degrade completely within several hours. Therefore, the micelles were able to unload LTG in response to oxidative stress, while maintaining integrity in normal environment.

3.3. *Cellular biocompatibility of materials*

As is well known, biocompatibility of the polymers should be firstly verified before any administration *in vivo*. SH-SY5Y cells

were selected to simulate neurons in testing the cellular compatibility of PLB, DPLB and DHAA. It was revealed that both polymers were rather safe for cell cultures below a concentration of 200 μg/mL (Supporting Information Fig. S13A). Moreover, as for DHAA, the safety limit was as high as 100 μg/mL (Fig. S13B). In preservation of cellular viability, it was assured that the cells would not be exposed to a concentration above the safety limits during the following cellular examinations. Meanwhile, when administered at the designed dosage, the plasma concentration of LTG *in vivo* would be profoundly lower than the safety limits. Therefore, the polymers should be biologically compatible in both cellular and animal studies.

3.4. Cellular uptake of micelles

As was reported before, glucose is heavily consumed in the normal brain, and more glucose is required and transported by GLUT1 (a typical membrane protein shown in Fig. S13C) in epileptic foci when early seizures occur[26−28]. Thus, we decorated the surface of the nano-medicine with GLUT1-targeting DHAA to enhance BBB penetration and cerebral accumulation. As a brain-targeting ligand, DHAA should firstly serve to promote cellular uptake. To investigate the relationship between DHAA-modification ratio and cellular uptake, different micelles loading coumarin-6 (Cou-6) were constituted by changing the relative amount of DPLB to PLB during rehydration. With the modification ratio increasing, intracellular uptake by BCECs and SH-SY5Y cells both increased. The positive correlation was prominent when modification ratio was below 20%, and less significant between 20% and 100% (Fig. 2A and Fig. S14). For a more accessible synthesis protocol, we comprehensively determined to modify 20% of all polymers constituting targeted micelles in the following experiments. Therefore, we further examined the cytotoxicity of non-targeted micelles (LTG@PLB) and targeted micelles (LTG@DPLB, composed of 80% PLB and 20% DPLB) in SH-SY5Y cells (Fig. 2B). We found that the concentration of both LTG@PLB and LTG@DPLB not higher than 200 μg/mL could ensure enough biosafety. Finally, we carefully decided to control all polymeric micelle solutions for administration not higher than 200 μg/mL.

To identify the internalization mechanism of the micelles, cellular uptake of LTG was measured under different inhibitory conditions[36]. To elaborate, phenylarsine oxide, filipin and colchicine were applied to inhibit clathrin-related endocytosis, caveolae-mediated endocytosis and macropinocytosis respectively. Meanwhile, a quantification scheme using HPLC was customized for LTG in cultured cells. Cell matrix and culture contents had little influence on the accuracy of quantification (Supporting Information Fig. S15A), and a sample recovery rate of 95.12 ± 4.61% was achieved. It was observed that colchicine seriously inhibited cellular internalization of LTG in BCECs while filipin heavily inhibited cellular uptake of LTG in SH-SY5Y cells (Fig. 2C and D). Thus, it is concluded that endothelial cells mainly internalized the micelles through micropinocytosis while neurons mainly absorbed the micelles through caveolae-mediated endocytosis. Intriguingly, phenylarsine oxide slightly inhibited cellular uptake of LTG in SH-SY5Y cells, suggesting an ancillary role of clathrin-related internalization of the micelles in neurons.

To investigate intracellular ROS-triggered release of micelles, SH-SY5Y cells incubated with Cou-6-loaded micelles were observed with laser confocal microscope under high power field. The microscopy showed that the micelles (green signals) had few parts of co-localization with endosomes/lysosomes (red signals), which supported the conclusion that targeting micelles entered the neurons mainly through caveolae-mediated endocytosis and partly through clathrin-dependent endocytosis (Fig. 2E). Green signals of Cou-6 experienced an acute increase upon ROS stimulation, demonstrating the micelles' ROS-sensitive degradation and cargo release intracellularly. By contrast, control groups in ROS-free conditions exhibited a weak fluorescence intensity stably over time, further proving that the micelles could degrade and unload the cargos distinctively in distinct response to oxidative stress.

The blockage of the BBB is one of the main difficulties in delivering drugs into the CNS, where almost all macromolecules and more than 98% of small molecules will be excluded by the BBB[9,37]. Therefore, we designed glucose analogue DHAA as the brain-targeting ligand of our preparation, in order to enhance cerebral penetration by way of GLUT1 on the BBB[38]. We cultured BCECs as monolayer in the Transwell inserts and established the BBB model *in vitro* (Fig. 2F)[39]. Before and after the experiment, the apparent permeability coefficients (P_{app}) of ^{14}C-labelled sucrose across the model were lower than 8×10^{-5} cm/s (Fig. S15B), which accorded with the permeability of complete monolayer cell reported before, indicating that the model was constructed successfully and remained intact in the experimental process[40]. We found that from 10 min after administration, the P_{app} of DHAA-modified micelles were significantly higher than those of non-modified micelles (Fig. 2G). This effect could be inhibited by the addition of excessive DHAA, which proved that the BBB penetration of our nano-medicine was mainly promoted by DHAA and GLUT1-mediated pathway. That, in turn, was consistent with the results of Fig. 2C.

3.5. Cellular protective effects of micelles

During epileptogenesis, harmful effects of oxidative stress directly come from ROS-mediated cellular injuries. Based on previous studies, SH-SY5Y cells were incubated with 100 μmol/L H_2O_2 to establish oxidative damage models that simulated the epileptic microenvironment[33,41,42]. Compared with the control group, H_2O_2-treated cells showed poor survival (Fig. 3A). By contrast, obvious increase in viability was observed in cells incubated with either LTG@DPLB micelles or DPLB micelles in advance. Meanwhile, free LTG only provided limited protection for H_2O_2-stimulated cells, indicating an indispensable role of the ROS-sensitive polymers in clearing ROS.

Ionotropic glutamate receptors would become susceptible to activation when focal glutamate concentration increased pathologically during epileptogenesis, which has been considered to be the direct cause of abnormal firing[1,13]. In addition, high concentration of glutamate could stimulate glial cells, aggravating the imbalance in glutamate metabolism. Consequently, there would form a vicious circle of glial activation, inflammatory reactions and oxidative stress. Allowing for the interactions involved, excitotoxicity models were established in SH-SY5Y cells through incubation with high glutamate concentration of 50 mmol/L, guided by previous studies[43−45]. Changes in cellular excitability after treatment with different preparations were characterized through whole-cell patch-clamp technique (Fig. 3B). By comparison with the control group, cells treated with 50 mmol/L glutamate showed apparent increase in excitability, especially under high clamp current (Fig. 3C). Furthermore, LTG@DPLB micelles gave the best performance in stabilizing the cells among different groups. Then, through flow cytometry analysis, it was

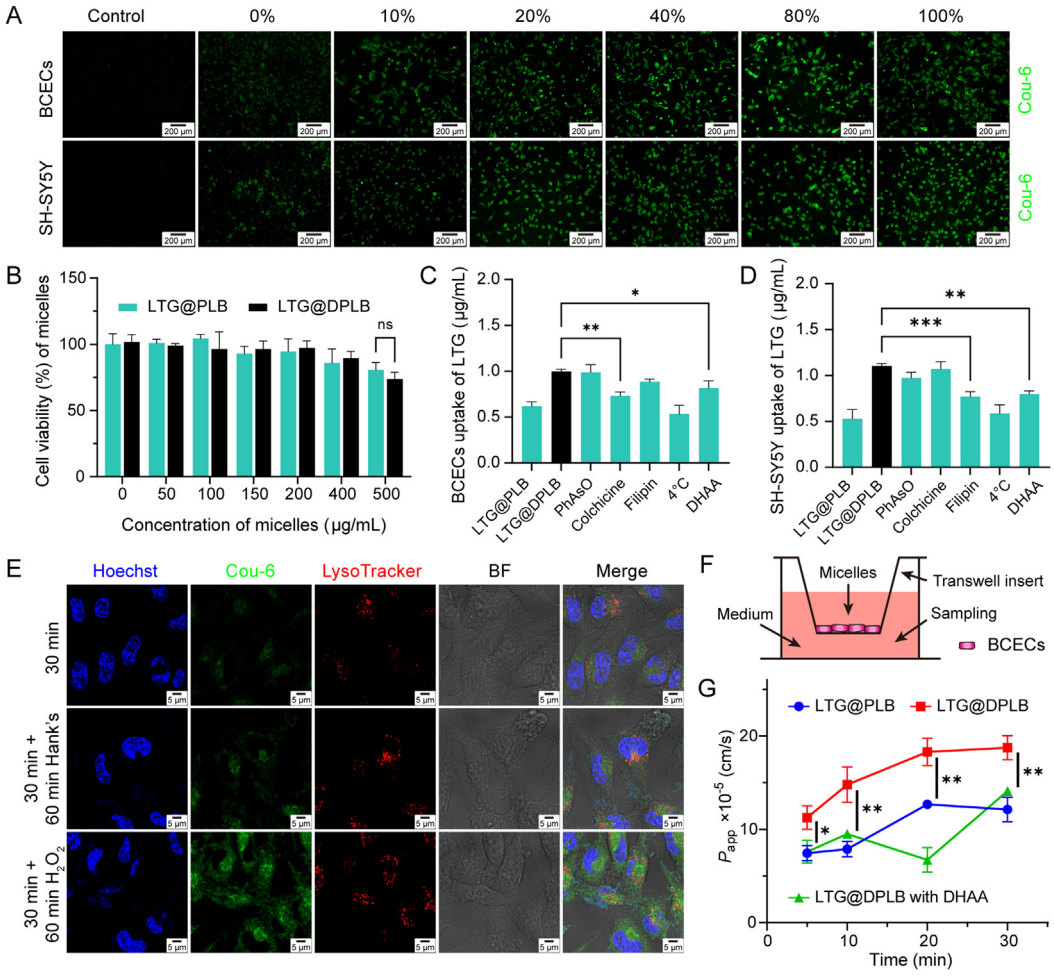

Figure 2 Cellular biocompatibility and uptake of micelles *in vitro*. (A) Cellular uptake of Cou-6-loaded micelles with different DHAA-modification ratios of 0%, 10%, 20%, 40%, 80% and 100% in BCECs and SH-SY5Y cells (scale bar: 200 μm; green signal: Cou-6); (B) Viability of SH-SY5Y cells incubated with different concentrations of non-targeted micelles (LTG@PLB) and targeted micelles (LTG@DPLB, composed of 80% PLB and 20% DPLB). Results are presented as mean ± SD ($n = 3$); (C,D) Quantitative cellular uptake of micelles in BCECs and SH-SY5Y cells treated with six different inhibitive conditions. Results are presented as mean ± SD ($n = 3$, $^{*}P < 0.05$, $^{**}P < 0.01$, $^{***}P < 0.001$); (E) Lysosomal escape and cellular drug release of micelles induced by 100 μmol/L H_2O_2 in SH-SY5Y cells (scale bar: 5 μm; blue signal: Hoechst; green signal: Cou-6; red signal: LysoTracker); (F) Illustration of the BCEC monolayer transwell system; (G) Quantitative transcytosis of LTG encapsulated in micelles across the BBB model *in vitro* (calculated as apparent permeability coefficients, or P_{app}). Data are presented as mean ± SD ($n = 3$, $^{*}P < 0.05$, $^{**}P < 0.01$).

observed that early apoptosis was suppressed in cells treated with LTG@DPLB micelles (Fig. 3D and E) while ROS-indicative staining results showed that LTG@DPLB micelles managed to scavenge ROS within SH-SY5Y cells (Fig. 3F and Supporting Information Fig. S15C−S15E). Therefore, it was concluded that LTG@DPLB micelles exhibited excellent ability in defending against excitotoxicity and restoring neural stability. In view of the fact that high concentration of glutamate would directly cause excitotoxicity, or generate oxidative stress along with abnormal calcium influx followed by cellular hyperexcitability, we believed that LTG uptake promoted by LTG@DPLB micelles and antioxidant effect provided by DPLB polymers gave LTG@DPLB better anti-excitotoxicity effect than other groups[43,46].

To further verify our targeted delivery strategy based on increased GLUT1-mediated transport of DHAA in epileptic foci, we quantitated LTG@DPLB internalization in hyperexcited SH-SY5Y cells (Fig. 3G). A significant increase of LTG uptake was found in hyperexcited SH-SY5Y cells than normal cells, which could be partly antagonized by excessive DHAA. In addition, we also measured the GLUT1 expression of SH-SY5Y cells before and after glutamate-stimulation by Western blot, whose change was not apparent (Fig. S13D). Therefore, we believed that increased LTG@DPLB internalization in hyperexcited cells was more associated with the change of GLUT1-mediated glucose intake rather than GLUT1 expression. Considering the high energy demand and glucose intake in epileptic foci, we predicted that our targeted delivery strategy would also take effect *in vivo*.

3.6. In vivo distribution and brain-targeting efficiency of micelles

Acute seizure models were successfully established to simulate temporal lobe epilepsy (TLE) on rats *via* classic lithium-pilocarpine induced kindling, and verified with Racine's

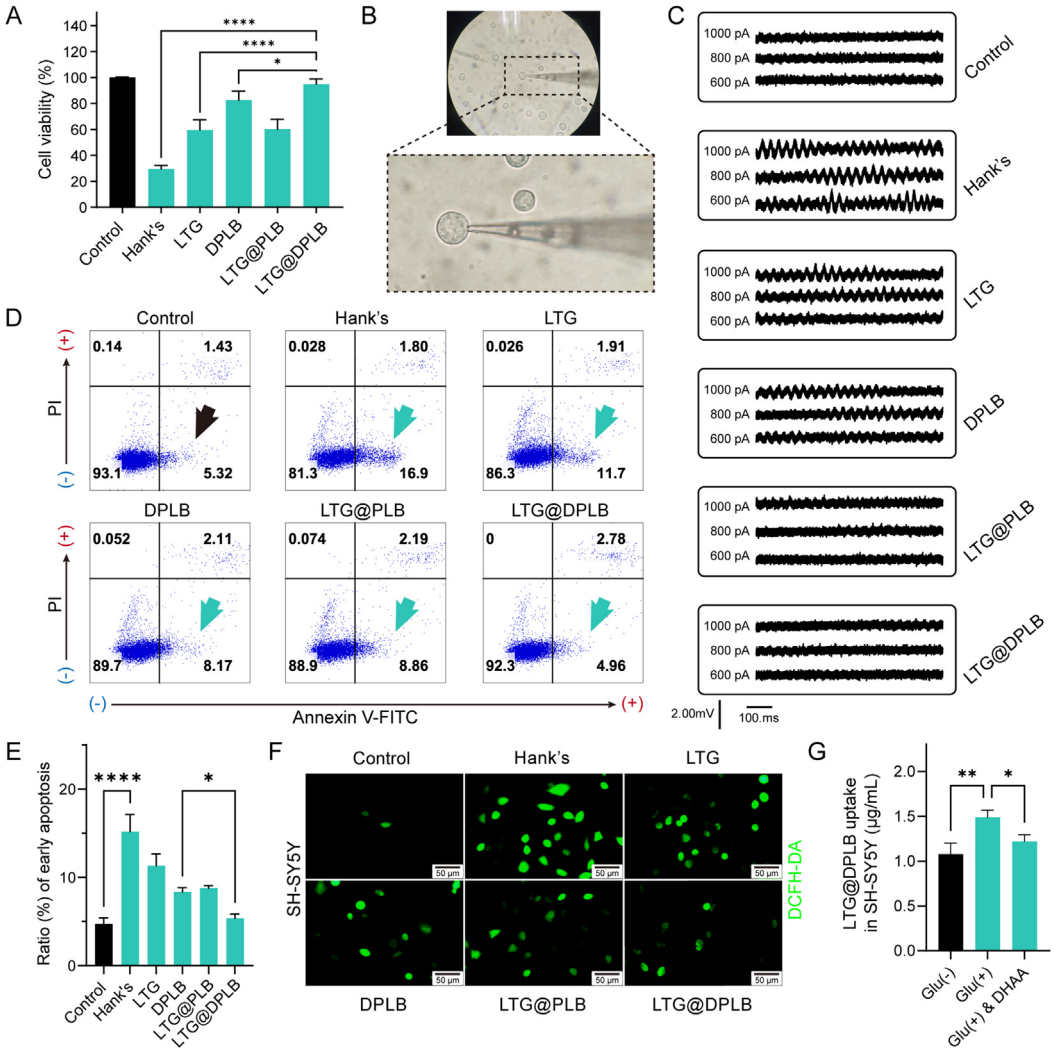

Figure 3 Neuroprotective effects of micelles on SH-SY5Y cells incubated with different neurotoxic conditions. (A) Viability of SH-SY5Y cells after incubation with 100 μmol/L H_2O_2. The cells were pre-treated with different preparations. Results are presented as mean ± SD ($n = 3$, $^*P < 0.05$, $^{****}P < 0.0001$); (B) The operation field and glass micropipette under arthroscopy of the whole-cell patch-clamp technique; in the center of the field, the glass microelectrode had sealed one cell. (C) Electrical activities of SH-SY5Y cells recorded by whole-cell patch-clamp with different compliance currents (600, 800 and 1000 pA); SH-SY5Y cells were cultured in 50 mmol/L glutamine to induce excitotoxicity and then treated with different preparations; (D) Flow cytometry analysis of excitotoxic cell apoptosis after treatment with different preparations; Positive signals of Annexin V-FITC with negative signals of propidium iodide (PI) (the fourth quadrant) directed the early apoptosis of SH-SY5Y cells; (E) Quantification of the cellular early apoptosis of SH-SY5Y cells analyzed by flow cytometry. Data are presented as mean ± SD ($n = 3$, $^*P < 0.05$, $^{****}P < 0.0001$); (F) ROS-staining of SH-SY5Y cells treated with different preparations against 50 mmol/L glutamine-induced excitotoxic injury (scale bar: 50 μm; green signal: DCFH-DA activated by ROS) (G) Quantitative cellular uptake of the targeted micelle (DPLB@LTG) in SH-SY5Y cells treated with glutamate (Glu)-stimulated [marked as Glu (+)] and even DHAA-inhibitive conditions. Results are calculated according to intracellular LTG and presented as mean ± SD ($n = 3$, $^*P < 0.05$, $^{**}P < 0.01$).

classification scale and electroencephalogram (EEG) records[47] (Supporting Information Figs. S16 and S17A). During acute seizures, improved penetration into the brain of common AEDs might represent better therapies against epilepsy with less adverse effects[48,49]. We expected these problems could be resolved by designing micelles modified with DHAA that could specifically target the brain. Therefore, BODIPY, a near-infrared probe whose fluorescence could highly penetrate subcutaneous tissue, was encapsulated in the micelles to indicate their *in vivo* distribution (Fig. S17B). BODIPY fluorescent signals in the head of tested rats were recorded by the IVIS® Spectrum *in vivo* imaging system (Fig. S17C). The fluorescence intensity within the brain area of the free BODIPY group (BODIPY) peaked 1 h after intravenous injection and did not increase thereafter (Fig. 4A). Meanwhile, the fluorescence intensity waned beyond 12 h after injection in the other three groups given micelles, confirming their long circulation effect *in vivo*. Besides, 4 h after intravenous injection, the signal from groups given targeted micelles (BODIPY@DPLB) showed a more prominent increase than that treated with free BODIPY or non-targeted micelles (BODIPY@PLB). We thereby preliminarily suggested that the targeted micelles might direct more cargos into the brain and an improved cerebral distribution

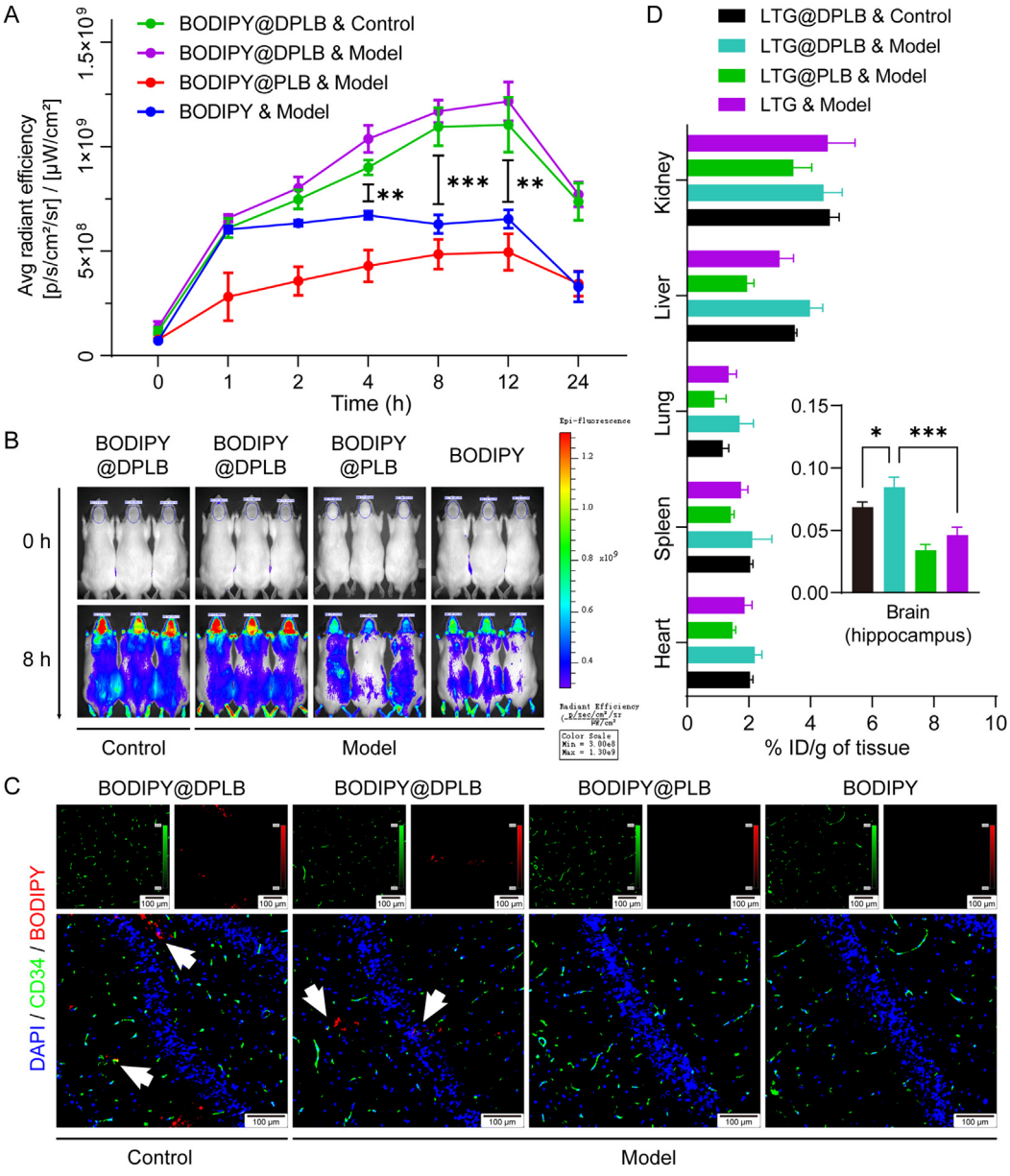

Figure 4 *In vivo* distribution study of micelles. (A) Semi-quantification of BODIPY fluorescent signals in the head analyzed by the IVIS software. Data are presented as mean ± SD ($n = 3$, $^{**}P < 0.01$, $^{***}P < 0.001$); (B) The IVIS Spectrum *in vivo* imaging of rats before and 8 h after injection with BODIPY or BODIPY-loaded micelles; (C) Distribution of BODIPY around vascular endothelial cells (stained with anti-CD34) in rat hippocampus 8 h after injection. White arrows indicate BODIPY-loaded micelles diffused away from blood vessels (scale bar: 100 μm; blue signal: DAPI; green signal: CD34; red signal: BODIPY); (D) Quantification of LTG distribution in different organs of different groups. The percentage of the injected dose per gram of tissue (% ID/g of tissue) was calculated according to HPLC results. Data are presented as mean ± SD ($n = 3$, $^{*}P < 0.05$, $^{***}P < 0.001$).

was seemingly realized. However, *in vivo* imaging results were not solid for lack of perfusion process. We next performed more detailed inspection of cerebral distribution.

Building upon the dynamic distribution obtained above, the 8th h post-injection was selected to be the time for further evaluation, when rats were perfused and brains were gathered to prepare frozen sections for immunofluorescence staining (Fig. 4B). CD34 was selected as a marker of vascular endothelial cells to determine cerebral BODIPY distribution (Fig. 4C). In the hippocampus of the rats given BODIPY@DPLB, a small part of red fluorescence signal representing BODIPY was co-located with green signal representing vascular endothelial cells, while most of the red signal was dispersed into brain parenchyma. However, no obvious red signal was observed in the hippocampus of those treated with free BODIPY or BODIPY@PLB, suggesting that targeted micelles could cross blood vessels and enter brain matter.

Moreover, rats were treated with free LTG or LTG-loaded micelles and 8 h post-injection, their brains (hippocampus) and major organs were gathered and assayed to determine the LTG content and calculate % ID/g of tissue (Fig. 4D). A quantification

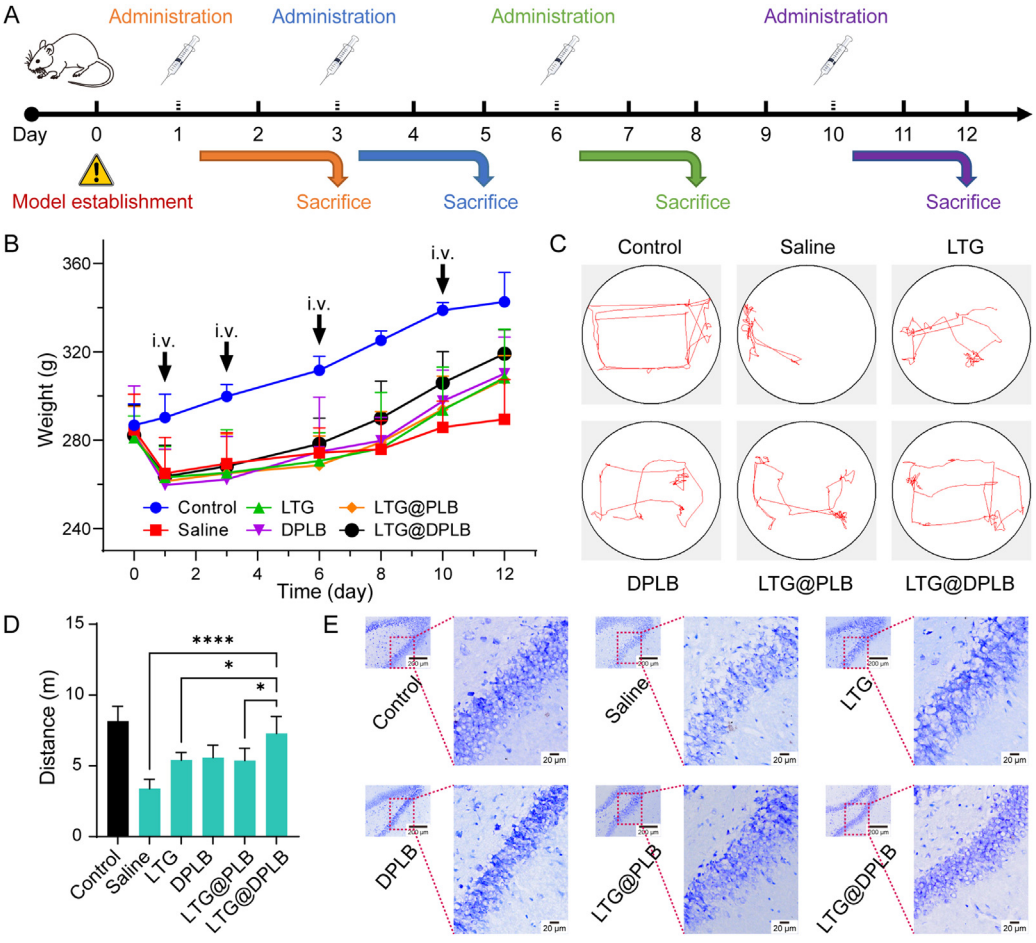

Figure 5 Rudimentary anti-epileptic efficacy study of micelles *in vivo*. (A) Treatment schedule; Epileptic rats were administered with different preparations on Days 1, 3, 6 and 10 after modeling; One day after each administration, rats were sacrificed to prepare samples for further analysis; (B) Weight of rats was recorded synchronously during the medication (before modeling and on Days 1,3, 6, 8, 10 and 12). Data are presented as mean ± SD (n = 20, 15, 10 or five at different time points); (C) The movement track of rats captured by Morris water maze camera for 1 min per group in open-field tests (Day 10); (D) Quantification of motion distance automatically calculated by Morris water maze software in open-field tests (Day 10). Results are presented as mean ± SD (n = 3, $^{*}P < 0.05$, $^{****}P < 0.0001$); (E) Nissl's staining of neurons' morphologic changes in rat hippocampus (scale bar: 200 μm for thumbnails and 20 μm for large images; mottled blue signal: Nissl's bodies; Day 10).

scheme specific for LTG in rat organs was established using HPLC, where tissue matrix or lysate buffer had little influence on the accuracy of the assay (Fig. S17D). The recoveries of LTG were 96.59 ± 1.18%, 93.25 ± 1.77%, 91.90 ± 2.35%, 89.42 ± 3.62%, 100.16 ± 3.25% and 88.43 ± 1.65% for heart, liver, spleen, lung, kidney and hippocampus, respectively, being suitable for quantification. We found that the quantitative result of ID/g (%) of brain was basically consistent with the semi-quantitative results of IVIS fluorescent imaging. It was also revealed that more LTG accumulated in the hippocampus of rats treated with LTG@DPLB micelles in comparison with those injected with free LTG or LTG@PLB micelles, suggesting that effective brain targeting was realized as designed. Besides, when both given LTG@DPLB micelles, the model group also showed enhanced LTG accumulation in hippocampus than the control group, which was consistent with the enhanced LTG@DPLB internalization in hyperexcited SH-SY5Y cells (Fig. 3G). In consideration of increased ictal glucose demand and internalization in epilepsy, we concluded that our GLUT1-targeting strategy is efficient to promote drug delivery into epileptic foci[50].

3.7. *In vivo anti-epileptic efficacy of micelles*

Epileptogenesis, if left uncontained at an early stage, would keep activating healthy glial cells and reinforcing the vicious cycle of inflammation, oxidative stress and gliosis. Eventually, epilepsy would turn refractory and damage neurons chronically[51]. Therefore, drug administration was repeated on the animal models at given intervals, in an effort to maintain the reclaimed homeostasis in local microenvironment. Samples were taken at least 1 day after every administration so that the drugs would have taken effect fully (Fig. 5A). A sharp decrease in the weights of model rats was observed after acute seizures were induced. Afterwards, the rats started to gain weight, where the LTG@DPLB group showed the fastest increase (Fig. 5B). Meanwhile, since generalized tonic clonic seizures put a great limitation on the mobility of modeled rats, open-field tests were performed after Day 10. We observed that the LTG@DPLB group showed similar travel patterns as the control while the saline-treated group was the most severely debilitated (Fig. 5C and D and Supporting Information Fig. S18A), and therefore, we terminated all administration. The

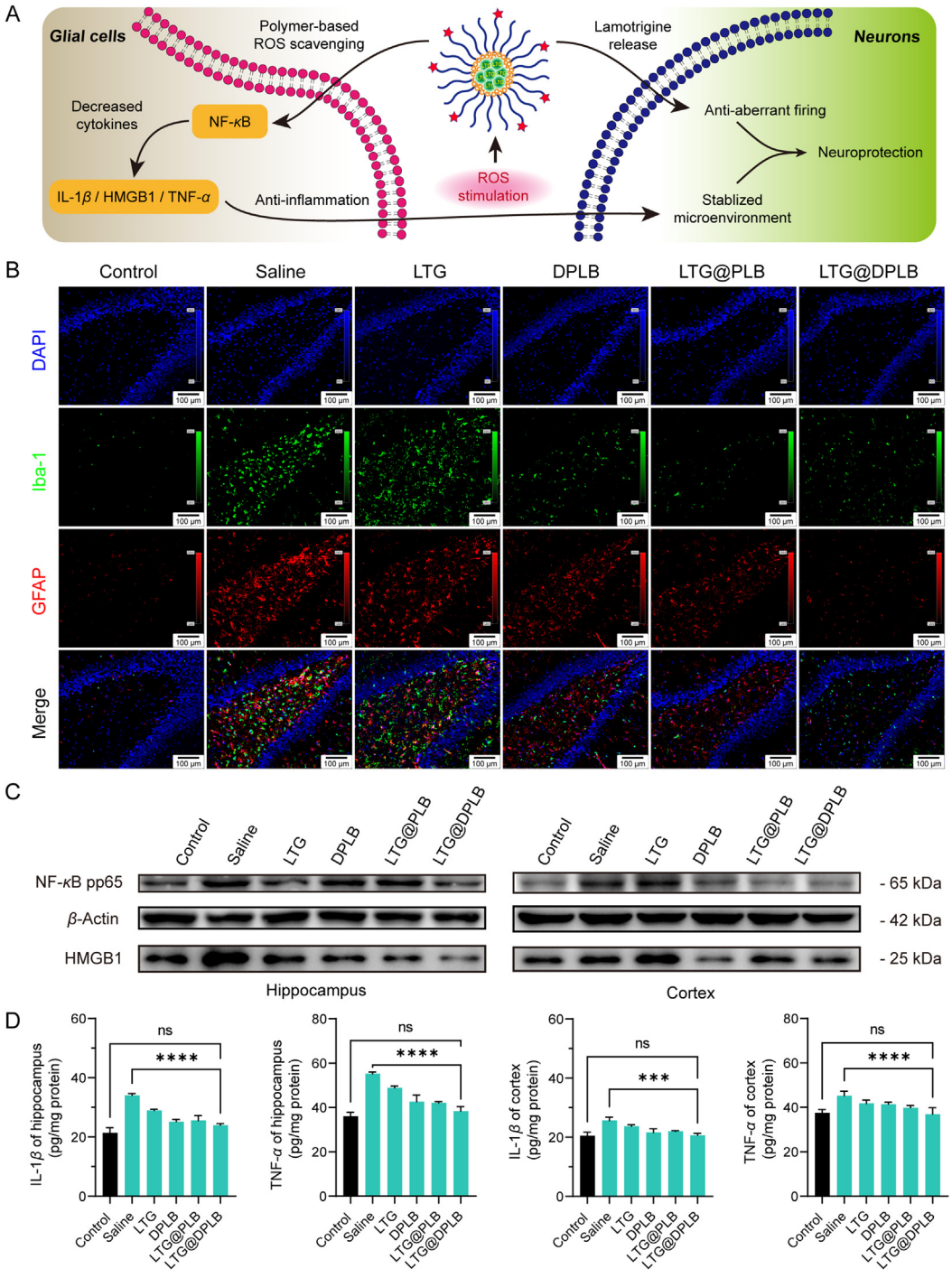

Figure 6 Advanced anti-epileptic efficacy study of micelles *in vivo*. (A) Illustration of epileptic inflammatory microenvironment and the therapeutic mechanism of the nano-medicine; (B) Immunofluorescence staining of reactive gliosis in rat hippocampus (scale bar: 100 μm; blue signal: DAPI; green signal: Iba-1; red signal: GFAP; Day 10); (C) Measurement of pro-inflammatory cytokines (NF-κB pp65 and HMGB1) in rat hippocampus and cortex (Day 10) by western blot (β-actin served as the inner parameter); (D) Measurement of pro-inflammatory cytokines (IL-1β and TNF-α) in rat hippocampus and cortex (Day 10) by enzyme-linked immunosorbent assay (ELISA). Results are presented as mean ± SD ($n = 3$, $^{***}P < 0.001$, $^{****}P < 0.0001$).

treatment lasted 12 days in total after model establishment, with four rounds of drug administration. It was preliminarily concluded that the LTG@DPLB group had the fastest recovery among the modeled groups.

Consecutive aberrant discharging during seizures would cause neuron damages, or even neuron death, which is normally evaluated with Nissl's staining[22,52]. After acute seizures were induced, misarrangement, deformation and vacuolar-like degeneration were observed in hippocampal neurons of all modeled rats, and sometimes neural loss could be viewed (Fig. 5E and S18B). As the treatment proceeded, neural protection happened the most obvious in LTG@DPLB group. After the 4th administration,

hippocampal neurons had restored normal morphology, tight arrangement and clear delineation in the LTG@DPLB group. At the meantime, scanning microscopy of the saline group could only capture few stained Nissl's bodies, suggesting widespread degeneration among the neurons. Though in the free LTG and the DPLB groups, much more Nissl's bodies were observed than the saline group, they still indicated misarrangement of the neurons. Therefore, we concluded that the LTG@DPLB micelles were the most capable of securing the neurons against damages or apoptosis.

Apart from neurons, neuroglia has been increasingly reported to be another important participant in epileptic micro-environment[53−55]. Alongside abnormally excited and impaired neurons are activated glial cells, excessive inflammatory factors and oxidative stress. Interactions among these factors eventually added up to an aggravating inflammatory microenvironment (Fig. 6A). Here, reactive gliosis, the continuous and excessive activation of neuroglia, was evaluated with immunofluorescence staining in the hippocampus of the rats. Iba-1 was selected as a marker of activated microglia, while GFAP was selected as a marker of reactive astrocytes. After acute seizures were induced, amoeboid microglia and hypertrophic astrocytes were observed to prevail while their resting states were inconspicuous, indicating intense activation of both microglia and astrocytes (Fig. S18C). As the treatment proceeded, gliosis decelerated in the LTG@DPLB group, and glial cells reverted to the similar conditions as the control after the 4th drug administration (Fig. 6B). By contrast, recovery was slower and unsustainable in other modeled groups (Fig. S18D and S18E). Therefore, LTG@DPLB micelles proved outstanding in ending the pathologically reactive gliosis and reclaiming glial homeostasis.

We further explored the biological mechanisms of neuro-protection and glial stabilization of the preparation in molecular terms. It was reported that pro-inflammatory factors related to epileptic inflammatory microenvironment mainly included interleukin-1β (IL-1β), high mobility group protein 1 (HMGB1), tumor necrosis factor-α (TNF-α), phosphorylated NF-κB p65 (NF-κB pp65), etc[56]. During epileptogenesis, reactive gliosis leads to the secretion of a variety of inflammatory factors and ROS, which in turn acts on the surrounding resting glial cells, causing more glial activation and continuous oxidative stress. Western blot (WB) and ELISA were performed to detect the expression of inflammatory factors in hippocampus and cortex of rats. After induction of acute seizures, WB observed a rapid upregulation of NF-κB pp65 and HMGB1 in the hippocampus (Supporting Information Fig. S19A). With the drug administration continuing, the expression of pro-inflammatory factors began to decline, where the LTG@DPLB group recovered the fastest, benefiting from continuous ROS clearance (Fig. 6C). In addition, ELISA experiments on the expression of IL-1β and TNF-α in the hippocampus also found a similar trend (Fig. 6D). For the cortex, we found that although the upregulation of these inflammatory factors was not as violent as that in the hippocampus, it was still obvious that LTG@DPLB could better inhibit the expression of pro-inflammatory factors. In brief, the targeted nano-medicine we designed could effectively inhibit pro-inflammatory factors in epileptic lesions and stabilize cerebral microenvironment (Fig. S19B).

At the end of the 12-day treatment, we briefly evaluated the biosafety of micelles *in vivo*. No obvious pathological changes were found in the results of hematoxylin-eosin (H&E) staining of different organs, which further indicated the biocompatibility of our preparation (Fig. S19C).

4. Conclusions

In this work, we prepared a brain-targeted nano-drug delivery system that could simultaneously inhibit abnormal discharges, reduce oxidative stress and regulate inflammatory microenvironment in cerebral foci for the early treatment of epilepsy. With the assistance of brain-targeting ligand DHAA, our micelles could penetrate the BBB and then release lamotrigine under the stimulation from high concentration of ROS in epileptic lesions. The vicious circle of aberrant firing, reactive gliosis, oxidative stress, chronic inflammation and neuronal injuries was effectively broken under the combined therapy of lamotrigine and ROS-scavenger phenylboronic ester, finally playing a role in protecting neurons and stabilizing glia. Compared with conventional AEDs, the nano-medicine we developed taken more pathological factors of epileptic lesions into account. Experimental results had confirmed that our preparation could make up for the deficiency of administering AEDs alone and promote recovery from seizures. Our preparation has the potential to serve as a novel strategy on early management of epilepsy.

Acknowledgments

We acknowledge the support from the National Natural Science Foundation of China (81872808, 82121002), Key Projects of Shanghai Science Founation (19JC1410800, China), and Shanghai Municipal Science and Technology Major Project (2018SHZDZX01, China) and ZJLab.

Author contributions

Chen Jiang, Tao Sun and Zheng Zhou conceived the concept of the study. Zheng Zhou, Keying Li, Yongchao Chu, Chao Li, Tongyu Zhang and Peixin Liu performed the experiments. Zheng Zhou and Keying Li wrote the manuscript.

Conflicts of interest

The authors declare no conflicts of interest.

Appendix A. Supporting information

Supporting data to this article can be found online at https://doi.org/10.1016/j.apsb.2022.09.019.

References

1. Patel DC, Tewari BP, Chaunsali L, Sontheimer H. Neuron-glia interactions in the pathophysiology of epilepsy. *Nat Rev Neurosci* 2019;**20**:282−97.
2. Diaz Verdugo C, Myren-Svelstad S, Aydin E, Van Hoeymissen E, Deneubourg C, Vanderhaeghe S, et al. Glia-neuron interactions underlie state transitions to generalized seizures. *Nat Commun* 2019;**10**:3830.
3. Vezzani A, Balosso S, Ravizza T. Neuroinflammatory pathways as treatment targets and biomarkers in epilepsy. *Nat Rev Neurol* 2019;**15**:459−72.
4. McElroy PB, Liang LP, Day BJ, Patel M. Scavenging reactive oxygen species inhibits status epilepticus-induced neuroinflammation. *Exp Neurol* 2017;**298**:13−22.
5. Drion CM, van Scheppingen J, Arena A, Geijtenbeek KW, Kooijman L, van Vliet EA, et al. Effects of rapamycin and curcumin on inflammation and oxidative stress *in vitro* and *in vivo*—in search of

potential anti-epileptogenic strategies for temporal lobe epilepsy. *J Neuroinflammation* 2018;**15**:212.
6. Shekh-Ahmad T, Lieb A, Kovac S, Gola L, Christian Wigley W, Abramov AY, et al. Combination antioxidant therapy prevents epileptogenesis and modifies chronic epilepsy. *Redox Biol* 2019;**26**:101278.
7. Johnson MR, Kaminski RM. A systems-level framework for anti-epilepsy drug discovery. *Neuropharmacology* 2020;**170**:107868.
8. Loscher W, Klein P. The feast and famine: epilepsy treatment and treatment gaps in early 21st century. *Neuropharmacology* 2020;**170**:108055.
9. Han H, Mann A, Ekstein D, Eyal S. Breaking bad: the structure and function of the blood−brain barrier in epilepsy. *AAPS J* 2017;**19**:973−88.
10. Cano A, Ettcheto M, Espina M, Auladell C, Calpena AC, Folch J, et al. Epigallocatechin-3-gallate loaded PEGylated-PLGA nanoparticles: a new anti-seizure strategy for temporal lobe epilepsy. *Nanomedicine* 2018;**14**:1073−85.
11. Ana R, Mendes M, Sousa J, Pais A, Falcao A, Fortuna A, et al. Rethinking carbamazepine oral delivery using polymer-lipid hybrid nanoparticles. *Int J Pharm* 2019;**554**:352−65.
12. Zhao J, Ye Z, Yang J, Zhang Q, Shan W, Wang X, et al. Nanocage encapsulation improves antiepileptic efficiency of phenytoin. *Biomaterials* 2020;**240**:119849.
13. Wang Y, Chen Z. An update for epilepsy research and antiepileptic drug development: toward precise circuit therapy. *Pharmacol Ther* 2019;**201**:77−93.
14. van Tienderen GS, Berthel M, Yue Z, Cook M, Liu X, Beirne S, et al. Advanced fabrication approaches to controlled delivery systems for epilepsy treatment. *Expet Opin Drug Deliv* 2018;**15**:915−25.
15. Mendez-Armenta M, Nava-Ruiz C, Juarez-Rebollar D, Rodriguez-Martinez E, Gomez PY. Oxidative stress associated with neuronal apoptosis in experimental models of epilepsy. *Oxid Med Cell Longev* 2014;**2014**:293689.
16. Gao F, Xiong Z. Reactive oxygen species responsive polymers for drug delivery systems. *Front Chem* 2021;**9**:649048.
17. Liu Y, Liu Y, Zang J, Abdullah AAI, Li Y, Dong H. Design strategies and applications of ros-responsive phenylborate ester-based nanomedicine. *ACS Biomater Sci Eng* 2020;**6**:6510−27.
18. Lu Y, Li C, Chen Q, Liu P, Guo Q, Zhang Y, et al. Microthrombus-targeting micelles for neurovascular remodeling and enhanced microcirculatory perfusion in acute ischemic stroke. *Adv Mater* 2019;**31**:e1808361.
19. Wang Y, Li L, Zhao W, Dou Y, An H, Tao H, et al. Targeted therapy of atherosclerosis by a broad-spectrum reactive oxygen species scavenging nanoparticle with intrinsic anti-inflammatory activity. *ACS Nano* 2018;**12**:8943−60.
20. Ammar HO, Ghorab MM, Mahmoud AA, Higazy IM. Lamotrigine loaded poly-varepsilon-(D,L-lactide-*co*-caprolactone) nanoparticles as brain delivery system. *Eur J Pharm Sci* 2018;**115**:77−87.
21. Alam T, Pandit J, Vohora D, Aqil M, Ali A, Sultana Y. Optimization of nanostructured lipid carriers of lamotrigine for brain delivery: *in vitro* characterization and *in vivo* efficacy in epilepsy. *Expet Opin Drug Deliv* 2015;**12**:181−94.
22. Liu J, He Y, Zhang J, Li J, Yu X, Cao Z, et al. Functionalized nanocarrier combined seizure-specific vector with P-glycoprotein modulation property for antiepileptic drug delivery. *Biomaterials* 2016;**74**:64−76.
23. Terstappen GC, Meyer AH, Bell RD, Zhang W. Strategies for delivering therapeutics across the blood−brain barrier. *Nat Rev Drug Discov* 2021;**20**:362−83.
24. Shao K, Zhang Y, Ding N, Huang S, Wu J, Li J, et al. Functionalized nanoscale micelles with brain targeting ability and intercellular microenvironment biosensitivity for anti-intracranial infection applications. *Adv Healthc Mater* 2015;**4**:291−300.
25. Cisternas P, Silva-Alvarez C, Martinez F, Fernandez E, Ferrada L, Oyarce K, et al. The oxidized form of vitamin C, dehydroascorbic acid, regulates neuronal energy metabolism. *J Neurochem* 2014;**129**:663−71.
26. Zhang Y, Xu J, Zhang K, Yang W, Li B. The anticonvulsant effects of ketogenic diet on epileptic seizures and potential mechanisms. *Curr Neuropharmacol* 2018;**16**:66−70.
27. Wasterlain CG, Fujikawa DG, Penix L, Sankar R. Pathophysiological mechanisms of brain damage from status epilepticus. *Epilepsia* 1993;**34 Suppl I**:S37−53.
28. Fulton RE, Pearson-Smith JN, Huynh CQ, Fabisiak T, Liang LP, Aivazidis S, et al. Neuron-specific mitochondrial oxidative stress results in epilepsy, glucose dysregulation and a striking astrocyte response. *Neurobiol Dis* 2021;**158**:105470.
29. Shi Y, Lu A, Wang X, Belhadj Z, Wang J, Zhang Q. A review of existing strategies for designing long-acting parenteral formulations: focus on underlying mechanisms, and future perspectives. *Acta Pharm Sin B* 2021;**11**:2396−415.
30. Jafari M, Doustdar F, Mehrnejad F. Molecular self-assembly strategy for encapsulation of an amphipathic alpha-helical antimicrobial peptide into the different polymeric and copolymeric nanoparticles. *J Chem Inf Model* 2019;**59**:550−63.
31. Faisal KS, Clulow AJ, Krasowska M, Gillam T, Miklavcic SJ, Williamson NH, et al. Interrogating the relationship between the microstructure of amphiphilic poly(ethylene glycol-*b*-caprolactone) copolymers and their colloidal assemblies using non-interfering techniques. *J Colloid Interface Sci* 2021;**606**:1140−52.
32. Winterbourn CC. Reconciling the chemistry and biology of reactive oxygen species. *Nat Chem Biol* 2008;**4**:278−86.
33. Arena A, Zimmer TS, van Scheppingen J, Korotkov A, Anink JJ, Muhlebner A, et al. Oxidative stress and inflammation in a spectrum of epileptogenic cortical malformations: molecular insights into their interdependence. *Brain Pathol* 2019;**29**:351−65.
34. Rios N, Radi R, Kalyanaraman B, Zielonka J. Tracking isotopically labeled oxidants using boronate-based redox probes. *J Biol Chem* 2020;**295**:6665−76.
35. Song S, Gao P, Sun L, Kang D, Kongsted J, Poongavanam V, et al. Recent developments in the medicinal chemistry of single boron atom-containing compounds. *Acta Pharm Sin B* 2021;**11**:3035−59.
36. Mazumdar S, Chitkara D, Mittal A. Exploration and insights into the cellular internalization and intracellular fate of amphiphilic polymeric nanocarriers. *Acta Pharm Sin B* 2021;**11**:903−24.
37. Han L, Jiang C. Evolution of blood−brain barrier in brain diseases and related systemic nanoscale brain-targeting drug delivery strategies. *Acta Pharm Sin B* 2021;**11**:2306−25.
38. Patching SG. Glucose transporters at the blood−brain barrier: function, regulation and gateways for drug delivery. *Mol Neurobiol* 2017;**54**:1046−77.
39. Khan NU, Ni J, Ju X, Miao T, Chen H, Han L. Escape from abluminal LRP1-mediated clearance for boosted nanoparticle brain delivery and brain metastasis treatment. *Acta Pharm Sin B* 2021;**11**:1341−54.
40. Santaguida S, Janigro D, Hossain M, Oby E, Rapp E, Cucullo L. Side by side comparison between dynamic *versus* static models of blood−brain barrier *in vitro*: a permeability study. *Brain Res* 2006;**1109**:1−13.
41. Das A, Belagodu A, Reiter RJ, Ray SK, Banik NL. Cytoprotective effects of melatonin on C6 astroglial cells exposed to glutamate excitotoxicity and oxidative stress. *J Pineal Res* 2008;**45**:117−24.
42. Pearson-Smith JN, Patel M. Metabolic dysfunction and oxidative stress in epilepsy. *Int J Mol Sci* 2017;**18**:2365.
43. Sarlo GL, Holton KF. Brain concentrations of glutamate and GABA in human epilepsy: a review. *Seizure* 2021;**91**:213−27.
44. Lukasiuk K, Pitkanen A. $GABA_A$-mediated toxicity of hippocampal neurons. *in vitro*. *J Neurochem* 2000;**74**:2445−54.
45. Santillo S. Changes in biophysical properties of undifferentiated SH-SY5Y cells during long-term cultures. *Neuroscience* 2022;**482**:143−58.
46. Mao XY, Zhou HH, Jin WL. Redox-related neuronal death and crosstalk as drug targets: focus on epilepsy. *Front Neurosci* 2019;**13**:512.
47. Cambiaghi M, Magri L, Cursi M. Importance of EEG in validating the chronic effects of drugs: suggestions from animal models of epilepsy treated with rapamycin. *Seizure* 2015;**27**:30−9.

48. Loscher W, Klitgaard H, Twyman RE, Schmidt D. New avenues for anti-epileptic drug discovery and development. *Nat Rev Drug Discov* 2013;**12**:757−76.
49. Loscher W, Potschka H. Drug resistance in brain diseases and the role of drug efflux transporters. *Nat Rev Neurosci* 2005;**6**:591−602.
50. Rho JM, Boison D. The metabolic basis of epilepsy. *Nat Rev Neurol* 2022;**18**:333−47.
51. Mao XY, Zhou HH, Jin WL. Redox-related neuronal death and crosstalk as drug targets: focus on epilepsy. *Front Neurosci* 2019;**13**:512.
52. Somani A, Zborovschi AB, Liu Y, Patodia S, Michalak Z, Sisodiya SM, et al. Hippocampal morphometry in sudden and unexpected death in epilepsy. *Neurology* 2019;**93**:e804−14.
53. Di Nunzio M, Di Sapia R, Sorrentino D, Kebede V, Cerovic M, Gullotta GS, et al. Microglia proliferation plays distinct roles in acquired epilepsy depending on disease stages. *Epilepsia* 2021;**62**:1931−45.
54. Shen Y, Qin H, Chen J, Mou L, He Y, Yan Y, et al. Postnatal activation of TLR4 in astrocytes promotes excitatory synaptogenesis in hippocampal neurons. *J Cell Biol* 2016;**215**:719−34.
55. Eastman CL, D'Ambrosio R, Ganesh T. Modulating neuroinflammation and oxidative stress to prevent epilepsy and improve outcomes after traumatic brain injury. *Neuropharmacology* 2020;**172**:107907.
56. Nass RD, Wagner M, Surges R, Holdenrieder S. Time courses of HMGB1 and other inflammatory markers after generalized convulsive seizures. *Epilepsy Res* 2020;**162**:106301.